Pressure-induced reemergence of superconductivity in topological insulator $Sr_{0.065}Bi_2Se_3$

Yonghui Zhou,[1,2] Xuliang Chen,[1,2] Ranran Zhang,[1] Jifeng Shao,[1] Xuefei Wang,[1,2] Chao An,[1,2] Ying Zhou,[1,2] Changyong Park,[3] Wei Tong,[1] Li Pi,[1,4] Zhaorong Yang,[1,2,4,*] Changjin Zhang,[1,4,†] and Yuheng Zhang[1,4]

[1]*High Magnetic Field Laboratory, Chinese Academy of Sciences and University of Science and Technology of China, Hefei 230026, China*

[2]*Key Laboratory of Materials Physics, Institute of Solid State Physics, Chinese Academy of Sciences, Hefei 230031, China*

[3]*High Pressure Collaborative Access Team, Geophysical Laboratory, Carnegie Institution of Washington, Argonne, Illinois 60439, USA*

[4]*Collaborative Innovation Center of Advanced Microstructures, Nanjing 210093, China*

(Received 9 March 2016; published 26 April 2016)

The recently discovered $Sr_xBi_2Se_3$ superconductor provides an alternative and ideal material base for investigating possible topological superconductivity. Here, we report that in $Sr_{0.065}Bi_2Se_3$, the ambient superconducting phase is gradually depressed upon the application of external pressure. At high pressure, a second superconducting phase emerges at above 6 GPa, with a maximum T_c value of ~8.3 K. The joint investigations of the high-pressure synchrotron x-ray diffraction and electrical transport properties reveal that the reemergence of superconductivity in $Sr_{0.065}Bi_2Se_3$ is closely related to the structural phase transition from an ambient rhombohedral phase to a high-pressure monoclinic phase around 6 GPa, and further to another high-pressure tetragonal phase above 25 GPa.

DOI: 10.1103/PhysRevB.93.144514

I. INTRODUCTION

Topological insulators and topological superconductors are new states of quantum matter which cannot be adiabatically connected to conventional insulators and superconductors [1–4]. Topological insulators are characterized by a full insulating gap in the bulk and gapless edge or surface states which are protected by time-reversal symmetry. In recent years, topological insulating materials have been theoretically predicted and experimentally observed in a variety of systems, including HgTe quantum wells, BiSb alloys, and $TlBiSe_2$ and Bi_2Te_3 (Bi_2Se_3, Sb_2Te_3) single crystals [5–7].

The concept of topological insulators can also be applied to superconductors, due to the direct analogy between topological band theory and superconductivity. Of major interest in the field of topological superconductivity is the realization of Majorana fermions, which are predicted to exist as protected bound states in topological superconductors [3]. In recent years, tremendous efforts have been made in order to realize a real topological superconducting material [8–13]. Among them, the Cu-intercalated $Cu_xBi_2Se_3$ has attracted much attention, because large-size bulk superconducting single crystals can be obtained. Various experimental works as well as theoretical analyses have been done, in order to reveal the novel physical properties in the $Cu_xBi_2Se_3$ system [14–20]. However, whether or not $Cu_xBi_2Se_3$ is a topological superconductor is still controversial. Recently, we found that an alternative compound, $Sr_xBi_2Se_3$, exhibits superconductivity with high superconducting volume fraction [21]. The following investigations have revealed that the atomic position of Sr in $Sr_xBi_2Se_3$ is completely different from that of Cu in $Cu_xBi_2Se_3$. That is, the copper atoms are intercalated in the weakly van der Waals bonded Se-Se layers, while most of the intercalated strontium atoms are located in the Se-Bi-Se-Bi-Se quintuple layer [22]. Furthermore, the $Sr_xBi_2Se_3$ compounds exhibit a well-separated topological surface state from the bulk bands [21–24]. These facts suggest that the $Sr_xBi_2Se_3$ compound exhibits interesting physical phenomena and could serve as an important material base for the investigation of topological-superconducting-related properties.

In this work, we perform a systematic study on the electronic transport properties and the structural evolution of $Sr_{0.065}Bi_2Se_3$ under high pressure. We find that the ambient superconducting phase in $Sr_{0.065}Bi_2Se_3$ is gradually depressed with the application of pressure. Noticeably, a pressure-induced superconducting phase emerges at high pressure. It is found that the reemergence of superconductivity and the structural phase transition in $Sr_{0.065}Bi_2Se_3$ are quite comparable with the high-pressure-induced superconductivity in the Bi_2Se_3 pristine topological insulator, despite of the fact that $Sr_{0.065}Bi_2Se_3$ is a superconductor at ambient pressure.

II. EXPERIMENT

Single crystals of $Sr_{0.065}Bi_2Se_3$ with typical dimensions of $3 \times 3 \times 0.5$ mm^3 used in this work have been reported previously [21]. High-pressure resistance measurements were conducted in a screw-pressure-type diamond anvil cell (DAC). Diamond anvils of 200 μm culets and a T301 stainless-steel gasket covered with a mixture of epoxy and fine cubic boron nitride (c-BN) powder were used for high-pressure transport measurements. The four-probe method was applied in the ab plane of single crystals with typical dimensions of $90 \times 40 \times 10$ μm^3. The magnetoresistance experiments under high pressure were performed on the Cell5 Water-Cooling Magnet of the High Magnetic Field Laboratory of the Chinese Academy of Sciences. The measurements were done using a field-sweeping method at fixed temperature. The maximum magnetic field was 33 T. High-pressure synchrotron radiation x-ray diffraction measurements were performed at 16BMD [25], HPCAT, Advanced Photon Source, Argonne National Laboratory. The as-grown single crystals were ground into fine powder for the x-ray diffraction experiments with a

*zryang@issp.ac.cn
†zcjin@ustc.edu.cn

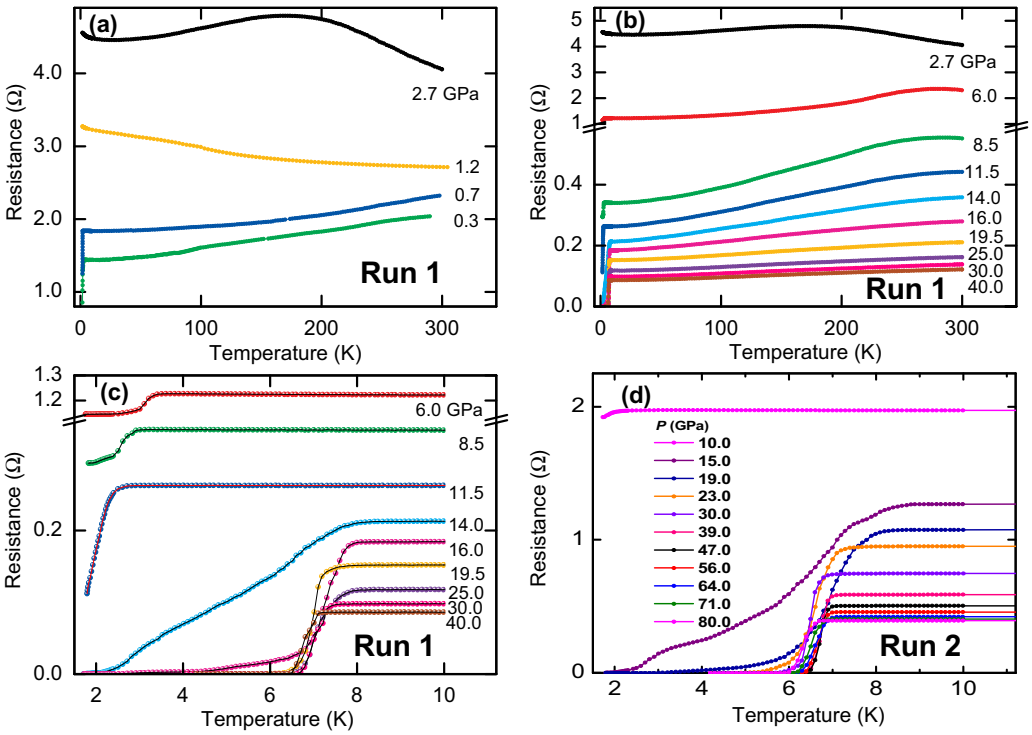

FIG. 1. (a) Temperature-dependent *ab*-plane resistance for $Sr_{0.065}Bi_2Se_3$ at low-pressure region. (b) Temperature-dependent *ab*-plane resistance for $Sr_{0.065}Bi_2Se_3$ at high-pressure region. (c) An enlarged view of the reemergent superconductivity near the transition temperature (run 1). (d) The temperature dependence of resistance for the $Sr_{0.065}Bi_2Se_3$ at run 2, reaching a maximum pressure of 80 GPa.

wavelength of 0.4246 Å. A rhenium gasket was preindented with a thickness of 40 μm. Then a 120 micrometer hole was drilled by the laser micromachining system at HPCAT [26], which served as a sample chamber. A prepressed powder sheet with a typical size of 30 μm × 30 μm × 15 μm was loaded into the chamber together with a ruby ball and silicone oil served as a pressure marker and pressure transmitting medium, respectively. A two-dimensional area detector Mar345 was used to collect the powder diffraction patterns. The DIOPTAS [27] and RIETICA [28] programs were employed for the image integrations and the XRD profile refinements, respectively. The Le Bail method was used to extract the lattice parameters. The pressure in the cell was measured at room temperature with an offline ruby system at HPCAT.

III. RESULTS AND DISCUSSION

Figure 1(a) gives the evolution of resistivity as a function of temperature for the $Sr_{0.065}Bi_2Se_3$ sample at relatively low pressure ($P \leqslant 3$ GPa). Two distinct features can be found in this pressure region. One is that the normal state resistivity increases with increasing pressure. The other is that the superconductivity is gradually depressed. If we compare the response of superconductivity of $Sr_{0.065}Bi_2Se_3$ with that of $Cu_{0.3}Bi_2Se_3$ [29], we find that the depression of superconductivity in the $Sr_{0.065}Bi_2Se_3$ sample is much faster than that in $Cu_{0.3}Bi_2Se_3$. The depression of superconductivity in $Sr_{0.065}Bi_2Se_3$ can be qualitatively explained according to a simple model for a low carrier density superconductor where $T_c \sim \Theta_D \exp[-1/N(0)V_0]$, with Θ_D the Debye temperature, $N(0) \sim m^* n^{1/3}$ the density of states (with m^* the effective mass), and V_0 the effective interaction parameter [29]. In $Sr_{0.065}Bi_2Se_3$, the reduction of charge carrier density n under pressure is apparent: The temperature dependence of resistivity gradually loses its metallic character with increasing pressure and the $\rho(300\ \mathrm{K})$ value exhibits an increase by a factor of >2 when the applied pressure is increased from 0.3 GPa to 2.7 GPa.

Figure 1(b) shows the temperature dependence of resistivity for the $Sr_{0.065}Bi_2Se_3$ sample with 2.7 GPa $\leqslant P \leqslant$ 40 GPa. It is interesting to notice that the normal state resistivity again exhibits a metallic-like feature, indicating an increase of charge carrier density at high pressure. The normal state resistivity decreases continuously with increasing pressure, suggesting a successive increase of charge carrier density at the high-pressure region. A striking phenomenon is that the $Sr_{0.065}Bi_2Se_3$ sample exhibits a reemergent superconductivity when $P \geqslant 6$ GPa. It should be mentioned that this reemergent superconductivity has not been observed in $Cu_xBi_2Se_3$ compounds. In order to see the reemergent superconductivity more clearly, we plot in Fig. 1(c) an enlarged view near the transition temperature. The T_c^{onset} value at 6.0 GPa is about 3.6 K. And the T_c^{onset} slightly decreases with increasing pressure when 6 GPa $\leqslant P \leqslant$ 11.5 GPa. However, when $P \geqslant 14$ GPa, the T_c^{onset} value is drastically increased, reaching a maximum of ~8.3 K. With further increasing pressure, the T_c^{onset} is slightly decreased. Nevertheless, the reemergent superconductivity of $Sr_{0.065}Bi_2Se_3$ is quite robust under high pressure. The superconductivity occurs even at the highest achieved pressure of 80 GPa [Fig. 1(d)]. We also notice that in iron chalcogenide superconductors, such as $Tl_{0.6}Rb_{0.4}Fe_{1.67}Se_2$, $K_{0.8}Fe_{1.7}Se_2$,

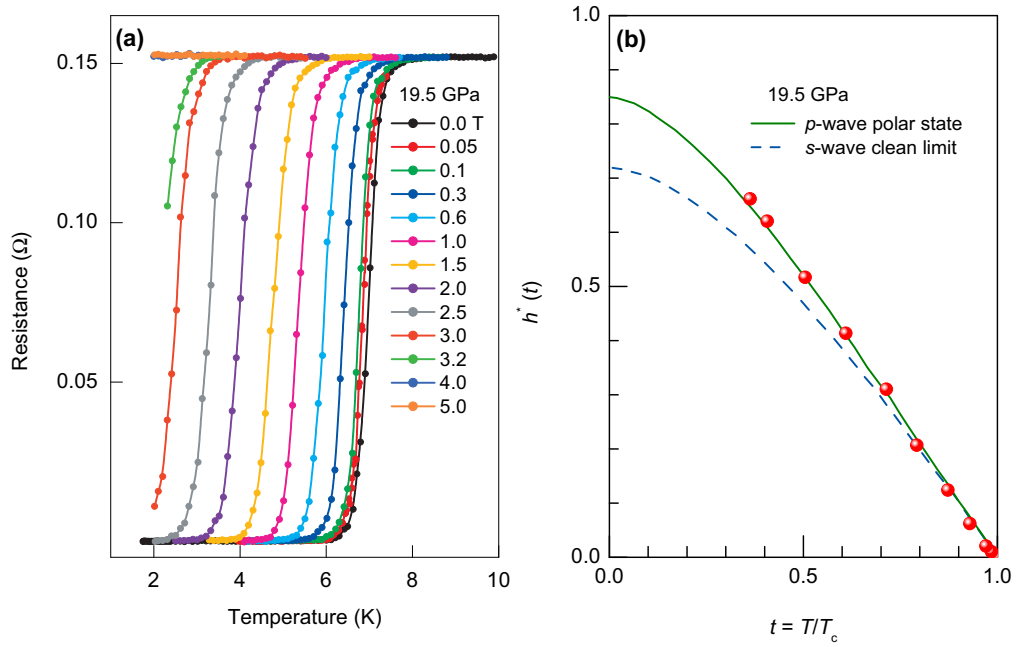

FIG. 2. (a) Temperature dependence of resistance under different magnetic fields up to 5.0 T. The applied pressure is fixed at 19.5 GPa. (b) Temperature dependence of the reduced upper critical field h^* (the red circles) and the fittings according to a p-wave polar state and the s-wave clean limit, respectively. The T_c at specific magnetic field is determined as a 90% drop of the normal state resistance.

and $K_{0.8}Fe_{1.78}Se_2$, the reemergent superconductivity with higher transition temperature has been reported [30]. However, in iron chalcogenides, the reemergent superconductivity occurs in a much narrower pressure range compared to the present case.

In order to tentatively estimate the nature of the reemergent superconductivity, we analyze the evolution of the upper critical field $H_{c2}(T)$ at low temperature. Figure 2(a) shows the response of the reemergent superconductivity on external magnetic field. The applied pressure is fixed at 19.5 GPa. It

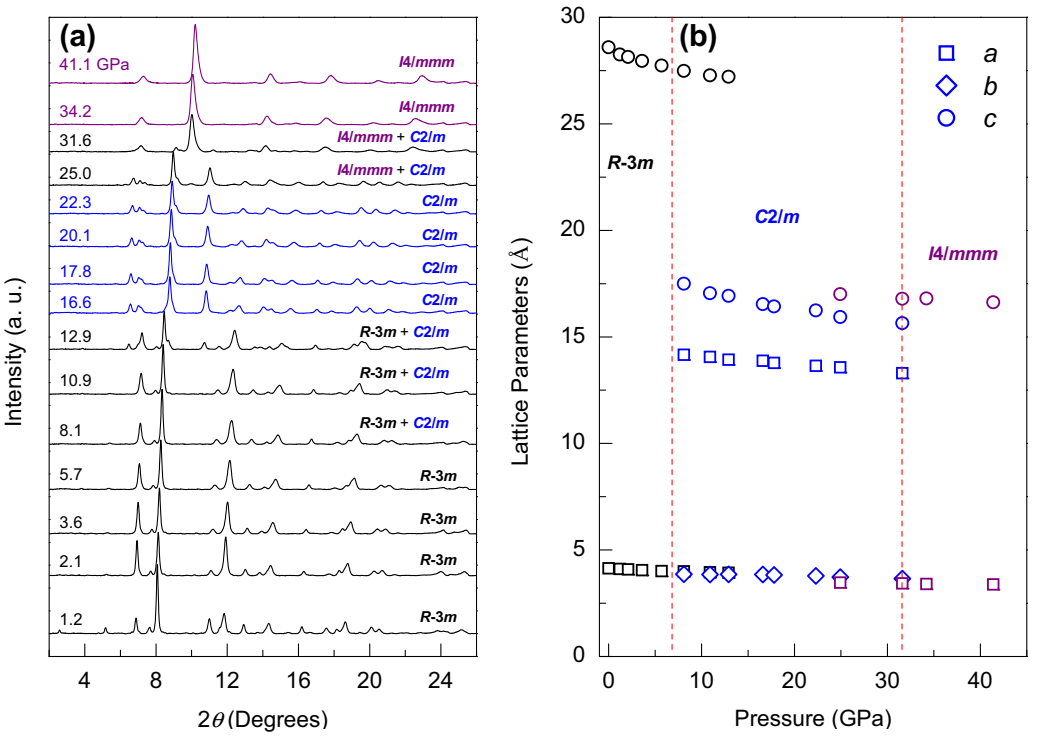

FIG. 3. (a) Synchrotron radiation x-ray diffraction patterns at various applied pressures. For clarity, the backgrounds have been subtracted by using the DIOPTAS program. (b) The refined lattice parameters a (squares), b (diamonds), and c (circles) as a function of pressure. Three structural phases, i.e., R-3m, $C2/m$, $I4/mmm$, with two overlap pressure regions are revealed upon compression.

is found that the superconducting transition temperature is monotonically decreased with increasing magnetic field. One striking feature is that both with and without magnetic field, the superconducting transition is rather sharp, meaning the occurrence of bulk and homogeneous superconductivity. It can be also found that the ρ-T curves are almost parallel to each other, suggesting that the flux creep effects can be completely ignored in the vortex dynamics of the reemergent superconductivity. Figure 2(b) plots the dependence of the reduced critical field, $h^*(T) = [H_{c2}(T)/T_c]/[dH_{c2}(T)/dT]|_{T=T_c}$, on the normalized temperature $t = T/T_c$. Here the $H_{c2}(T)$ value is defined from the resistance criterion of $R_{cri} = 90\%R_n$ (R_n is the normal state resistance). The experimental data are compared to models for orbitally limited s-wave and spin-triplet p-wave superconductors. It can be seen that the experimental $h^*(T)$ deviates significantly from the expected orbital-limited behavior predicted by the Werthamer-Helfand-Hohenberg (WHH) theory for an s-wave superconductor [$h^*(0) \simeq 0.72$] [31]. Noticeably, the $h^*(T)$ data are very close to the $h^*(T) \sim t$ curve expected from a p-wave superconductor [$h^*(0) \simeq 0.85$] [32]. We also note that a better fitting of the $h^*(T)$ data to a p-wave model rather than an s-wave model has been reported in pressure-induced superconductivity in the Bi_2Se_3 compound [33], pointing to unconventional superconductivity in the $Sr_xBi_2Se_3$ system.

It is instructive to investigate the structural symmetry at high pressure. Thus we conduct the high-pressure synchrotron x-ray diffraction (XRD) study on the $Sr_{0.065}Bi_2Se_3$ sample up to 41.1 GPa. In Fig. 3, the powder diffraction patterns and the lattice parameters under high pressure are presented in detail. Selected XRD profile refinements are also shown in Fig. 3. It is found that the ambient rhombohedral phase (R-3m) can remain in a single phase only when $P \leqslant 5.7$ GPa, above which a monoclinic phase ($C2/m$) is involved and coexists with the rhombohedral one. The low-pressure R-3m phase disappears completely at 16.6 GPa and the $C2/m$ phase persists up to 31.6 GPa. In the pressure range of 25.0–31.6 GPa, a mixture of the $C2/m$ phase and the high-pressure body-centered tetragonal phase ($I4/mmm$) shows up. Upon further compression beyond 31.6 GPa, the $I4/mmm$ phase can be sustained alone up to the highest pressure achieved in the present experiment.

To obtain a comprehensive understanding of the pressure-driven superconducting behavior, we show the isothermal equations of state for the respective phases in Fig. 4. The isothermal equations of state are fitted by the third-order Birch-Murnaghan formula [34] as indicated by the red solid lines in Fig. 4(a). With B_0' fixed as 4, the isothermal bulk modulus B_0 is estimated to be $\sim$ 58(1), 85(1), and 116(2) GPa for the R-3m, $C2/m$, and $I4/mmm$ phases, respectively. It is found that at the two progressive structural transition points (R-3$m \rightarrow C2/m \rightarrow I4/mmm$), the unit-cell volume per chemical formula ($Sr_{0.065}Bi_2Se_3$) shrinks by about 4.8% and 4.0%, respectively. According to the structural symmetries under high pressure, the superconducting phase diagram can be divided into two different regions as shown in Fig. 4(b): the pristine superconducting phase SC-I and the pressure-induced superconducting phase SC-II at high pressure. In the first region, the superconductivity is gradually depressed with increasing pressure. The T_c value approaches zero at an extrapolated pressure of about 1.1 GPa. Note that within this

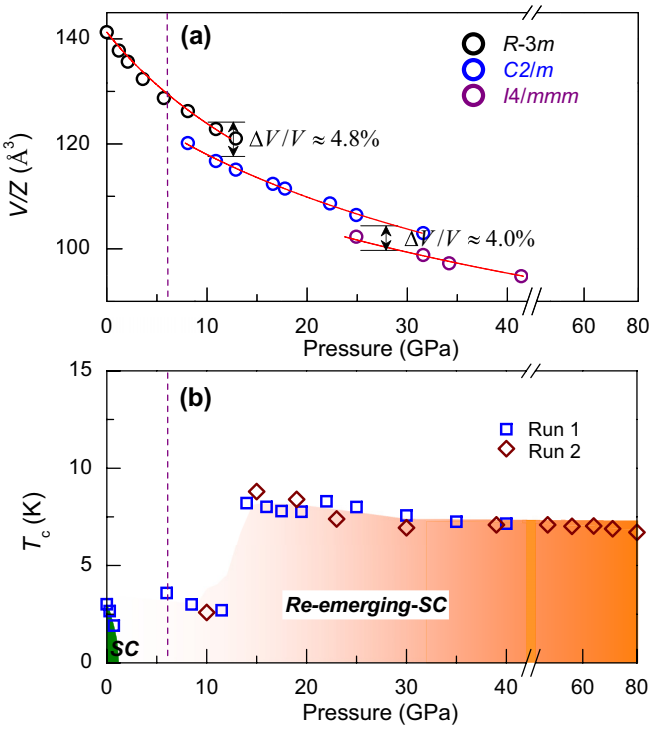

FIG. 4. (a) The compression data (V versus P) were fitted by the third-order Birch-Murnaghan equation of state (solid red line), which yields the bulk modulus 58(1), 85(1), 116(2) GPa for the R-3m, $C2/m$, and $I4/mmm$ phases, respectively. (b) The pristine superconducting phase, SC-I, occurs in the ambient rhombohedral (R-3m) phase. The reemergent superconducting phase, SC-II, occurs in the monoclinic ($C2/m$) phase and in the tetragonal $I4/mmm$ phase.

pressure range, the crystal structure of $Sr_{0.065}Bi_2Se_3$ is in the rhombohedral R-3m phase without structural phase transition. With increasing pressure, the $C2/m$ phase is involved and coexists with the rhombohedral R-3m phase. Meanwhile, the reemergent superconductivity occurs above 6 GPa. The superconducting critical temperature first experiences a tiny decrement till about 12 GPa. Then the R-3m phase disappears completely, leaving the $C2/m$ one staying alone. At the same time, the superconducting transition temperature jumps abruptly and reaches rapidly a maximum value of $\sim$8.3 K, which is followed by a slight decrease again. Upon further compression, the $C2/m$ to $I4/mmm$ structural phase transition occurs at around 25 GPa. As a matter of fact, previous high-pressure studies on Bi_2Se_3 have revealed a similar structural transition from the ambient-pressure rhombohedral (R-3m) structure to a lower-symmetry monoclinic ($C2/m$) structure near 10 GPa, and then to an unknown phase above 28 GPa [33,35]. Thus the structural phase transition in $Sr_{0.065}Bi_2Se_3$ at high pressure is similar to that in the Bi_2Se_3 pristine topological insulator.

IV. CONCLUSION

In conclusion, a pressure-induced reemergent superconductivity has been revealed in the $Sr_xBi_2Se_3$ superconducting topological insulator. The resulting phase diagrams exhibit

similar features to those of the high-pressure response of the Bi_2Se_3 pristine topological insulator, including the role of structural transitions and the presence of unconventional superconductivity. The analysis on the pressure-invariant T_c suggests the unconventional nature of the superconductivity in $Sr_xBi_2Se_3$, which deserves further investigation.

ACKNOWLEDGMENTS

This work was supported by the National Natural Science Foundation of China (Grants No. U1532267, No. U1332143, and No. 11574323). A portion of this work was performed on the WM5 magnet of the High Magnetic Field Laboratory, Chinese Academy of Sciences. Portions of this work were performed at HPCAT (Sector 16), Advanced Photon Source (APS), Argonne National Laboratory (ANL). HPCAT operations are supported by DOE-NNSA under Award No. DE-NA0001974 and DOE-BES under Award No. DE-FG02-99ER45775, with partial instrumentation funding by NSF. APS is supported by DOE-BES, under Contract No. DE-AC02-06CH11357.

Y. H. Zhou and X. L. Chen contributed equally to this work.

[1] C. L. Kane and E. J. Mele, Phys. Rev. Lett. **95**, 146802 (2005).
[2] B. A. Bernevig, T. L. Hughes, and S. C. Zhang, Science **314**, 1757 (2006).
[3] L. Fu and C. L. Kane, Phys. Rev. Lett. **100**, 096407 (2008).
[4] X. L. Qi and S. C. Zhang, Rev. Mod. Phys. **83**, 1057 (2011).
[5] M. König, S. Wiedmann, C. Brüne, A. Roth, H. Buhmann, L. W. Molenkamp, X.-L. Qi, and S.-C. Zhang, Science **318**, 766 (2007).
[6] D. Hsieh, D. Qian, L. Wray, Y. Xia, Y. S. Hor, R. J. Cava, and M. Z. Hasan, Nature (London) **452**, 970 (2008).
[7] H. J. Zhang, C.-X. Liu, X.-L. Qi, X. Dai, Z. Fang, and S.-C. Zhang, Nat. Phys. **5**, 438 (2009).
[8] Y. S. Hor, A. J. Williams, J. G. Checkelsky, P. Roushan, J. Seo, Q. Xu, H. W. Zandbergen, A. Yazdani, N. P. Ong, and R. J. Cava, Phys. Rev. Lett. **104**, 057001 (2010).
[9] M. Kriener, K. Segawa, Z. Ren, S. Sasaki, and Y. Ando, Phys. Rev. Lett. **106**, 127004 (2011).
[10] J. L. Zhang, S. J. Zhang, H. M. Weng, W. Zhang, L. X. Yang, Q. Q. Liu, S. M. Feng, X. C. Wang, R. C. Yu, L. Z. Cao, L. Wang, W. G. Yang, H. Z. Liu, W. Y. Zhao, S. C. Zhang, X. Dai, Z. Fang, and C. Q. Jin, Proc. Natl. Acad. Sci. USA **108**, 24 (2011).
[11] M. X. Wang, C. H. Liu, J.-P. Xu, F. Yang, L. Miao, M.-Y. Yao, C. L. Gao, C. Y. Shen, X. C. Ma, X. Chen, Z.-A. Xu, Y. Liu, S.-C. Zhang, D. Qian, J.-F. Jia, and Q.-K. Xue, Science **336**, 52 (2012).
[12] P. Zareapour, A. Hayat, S. Y. F. Zhao, M. Kreshchuk, A. Jain, D. C. Kwok, N. Lee, S.-W. Cheong, Z. Xu, A. Yang, G. D. Gu, S. Jia, R. J. Cava, and K. S. Burch, Nat. Commun. **3**, 1056 (2012).
[13] J. P. Xu, C. Liu, M.-X. Wang, J. Ge, Z.-L. Liu, X. Yang, Y. Chen, Y. Liu, Z.-A. Xu, C.-L. Gao, D. Qian, F.-C. Zhang, and J.-F. Jia, Phys. Rev. Lett. **112**, 217001 (2014).
[14] L. Fu and E. Berg, Phys. Rev. Lett. **105**, 097001 (2010).
[15] L. A. Wray, S.-Y. Xu, Y. Xia, Y. S. Hor, D. Qian, A. V. Fedorov, H. Lin, A. Bansil, R. J. Cava, and M. Z. Hasan, Nat. Phys. **6**, 855 (2010).
[16] S. Sasaki, M. Kriener, K. Segawa, K. Yada, Y. Tanaka, M. Sato, and Y. Ando, Phys. Rev. Lett. **107**, 217001 (2011).
[17] B. J. Lawson, Y. S. Hor, and L. Li, Phys. Rev. Lett. **109**, 226406 (2012).
[18] T. H. Hsieh and L. Fu, Phys. Rev. Lett. **108**, 107005 (2012).
[19] N. Levy, T. Zhang, J. Ha, F. Sharifi, A. A.Talin, Y. Kuk, and J. A. Stroscio, Phys. Rev. Lett. **110**, 117001 (2013).
[20] X. Wan and S. Y. Savrasov, Nat. Commun. **5**, 4144 (2014).
[21] Z. Liu, X. Yao, J. Shao, M. Zuo, L. Pi, S. Tan, C. Zhang, and Y. Zhang, J. Am. Chem. Soc. **137**, 10512 (2015).
[22] C. Q. Han, H. Li, W. J. Chen, F. Zhu, M.-Y. Yao, Z. J. Li, M. Wang, B. F. Gao, D. D. Guan, C. Liu, C. L. Gao, D. Qian, and J.-F. Jia, Appl. Phys. Lett. **107**, 171602 (2015).
[23] Shruti, V. K. Maurya, P. Neha, P. Srivastava, and S. Patnaik, Phys. Rev. B **92**, 020506(R) (2015).
[24] M. Neupane, Y. Ishida, R. Sankar, J.-X. Zhu, D. S. Sanchez, I. Belopolski, S.-Y. Xu, N. Alidoust, M. M. Hosen, S. Shin, F. Chou, M. Zahid Hasan, and T. Durakiewicz, Sci. Rep. **6**, 22557 (2016).
[25] C. Park, D. Popov, D. Ikuta, C. L. Lin, C. Kenney-Benson, E. Rod, A. Bommannavar, and G. Y. Shen, Rev. Sci. Instrum. **86**, 072205 (2015).
[26] R. Hrubiak, S. Sinogeikin, E. Rod, and G. Shen, Rev. Sci. Instrum. **86**, 072202 (2015).
[27] C. Prescher and V. B. Prakapenka, High Press. Res. **35**, 223 (2015).
[28] B. A. Hunter, Rietica—A Visual Rietveld Program, International Union of Crystallography Commission on Powder Diffraction Newsletter No. 20 (Summer 1998), http://www.rietica.org.
[29] T. V. Bay, T. Naka, Y. K. Huang, H. Luigjes, M. S. Golden, and A. de Visser, Phys. Rev. Lett. **108**, 057001 (2012).
[30] L. L. Sun, X.-J. Chen, J. Guo, P. Gao, Q.-Z. Huang, H. Wang, M. Fang, X. L. Chen, G. Chen, Q. Wu, C. Zhang, D. Gu, X. Dong, L. Wang, K. Yang, A. Li, X. Dai, H.-K. Mao, and Z. X. Zhao, Nature (London) **483**, 67 (2012).
[31] N. R. Werthamer, E. Helfand, and P. C. Hohenberg, Phys. Rev. **147**, 295 (1966).
[32] K. Scharnberg and R. A. Klemm, Phys. Rev. B **22**, 5233 (1980).
[33] K. Kirshenbaum, P. S. Syers, A. P. Hope, N. P. Butch, J. R. Jeffries, S. T. Weir, J. J. Hamlin, M. B. Maple, Y. K. Vohra, and J. Paglione, Phys. Rev. Lett. **111**, 087001 (2013).
[34] F. Birch, Phys. Rev. **71**, 809 (1947).
[35] R. Vilaplana, D. Santamaría-Pérez, O. Gomis, F. J. Manjón, J. González, A. Segura, A. Muñoz, P. Rodríguez-Hernández, E. Pérez-González, V. Marín-Borrás, V. Muñoz-Sanjose, C. Drasar, and V. Kucek, Phys. Rev. B **84**, 184110 (2011).